Elucidating the Redox Cycle of Environmental Phosphorus Using Ion Chromatography

Herbe Pech[1], Maria G. Vazquez[1], Jean Van Buren[1], Lixin Shi[2], Michelle M. Ivey[3], Tina M. Salmassi[2], Matthew A. Pasek[4], and **Krishna L. Foster[1,*]**

[1]Department of Chemistry and Biochemistry, California State University, Los Angeles 90032; [2]Department of Biological Sciences, California State University, Los Angeles 90032; [3]Harriet L. Wilkes Honors College, Florida Atlantic University, Jupiter 33458; [4]Department of Geology, University of South Florida, Tampa 33620

Abstract

Historically, it was assumed that reactive, inorganic phosphorus present in pristine environments was solely in the form of orthophosphate. However, this assumption contradicts theories of biogenesis and the observed metabolic behavior of select microorganisms. This paper discusses the role of ion chromatography (IC) in elucidating the oxidation-reduction cycle of environmental phosphorus. These methods employ suppressed-IC, coupled with tandem conductivity and electrospray mass spectrometry detectors to identify and quantify phosphorus oxyanions in natural water, synthetic cosmochemical, and biological samples. These techniques have been used to detect phosphite and orthophosphate in geothermal hot springs. Hypophosphite, phosphite, and orthophosphate have been detected in synthetic schreibersite corrosion samples, and termite extract supernatant. Synthetic schreibersite corrosion samples were also analyzed for two poly-phosphorus compounds, hypophosphate and pyrophosphate, and results show these samples did not contain concentrations above the 1.3 and 2.0 µM respective 3σ limit of detection. These methods are readily adaptable to a variety of matrices, and contribute to the elucidation of the oxidation-reduction cycle of phosphorus oxyanions in the environment. In contrast to most studies, these techniques have been used to show that phosphorus actively participates in redox processes in both the biological and geological world.

Introduction

Phosphate is an essential component of numerous compounds associated with life including the DNA backbone and phospholipids. Nevertheless, direct evidence to support theories on the origins of water soluble, reactive phosphorus oxyanions as precursors to organophosphates is sparse. One possible route that may lead to the formation of these compounds is the utilization of reduced oxidation state phosphorus compounds such as phosphite and hypophosphite. Indeed, microorganisms such as *Desulfotignum phosphitoxidans* have been identified with the ability to utilize the energy produced in the reduction of phosphite by sulfate for metabolism (1,2), and a multitude of other organisms are capable of using phosphite as their sole phosphorus source (3). The ability of these primitive organisms to utilize phosphite indicates that phosphite may have been present on ancient Earth. The detection of phosphite in primitive systems on modern-day earth may elucidate the mechanisms by which phosphorus transformed in pre-biota from a mineral into a biologically active form.

One possible route that may have led to reduced phosphorus oxyanions entering the biosphere is the aqueous corrosion of the meteoritic mineral schreibersite, $(Fe,Ni)_3P$, a mixed iron-nickel phosphide (4–6). The vast majority of elemental phosphorus on ancient Earth was stored in phosphate minerals (7), and apatite remains the greatest reservoir of phosphorus in the Earth's crust today (8–11). Calcium phosphate present in apatite stores phosphorus in the +5 oxidation state, and is not readily soluble in water. Unlike the Earth's phosphorus reservoir, calcium apatite, schreibersite readily corrodes in aqueous solutions into mixed valence states including hypophosphite (+1 oxidation state), phosphite (+3 oxidation state), diphosphite (+3 oxidation state), hypophosphate (+4 oxidation state), orthophosphate (+5 oxidation state), and pyrophosphate (+5 oxidation state). Recent studies have evaluated the role of atmospheric and solution compositions on the yields of specific valence states (12). The present study expands this work by addressing the roles of temperature, pH, and salinity.

Another possible route to the introduction of reduced phosphorus oxyanions to the early Earth is through volcanic activity and lightning storms. These high-energy conditions may have perturbed the thermodynamic equilibrium and reduced the oxidized state of inorganic phosphorus stored in minerals, which caused the element to become water soluble. Subsequently, reduced phosphorus compounds were oxidized to form polyphosphates found in biomolecules (13). Gulick proposed a radical concept that reduced phosphorus oxyanions such as hypophosphite (+1 oxidation state) and phosphite (+3 oxidation state) may play a critical role in the activation of phosphorus for use in biological systems (5). Lightning storms, especially those associated with volcanic activity, may have transformed the fully-oxidized phosphorus in apatite into reduced phosphorus compounds, including gaseous phosphine (14,15), hypophosphite

*Author to whom correspondence should be addressed: email kfoster@calstatela.edu.

(16,17), and phosphite (16,17). Calcium phosphite salts are approximately 1000 times more soluble in water than calcium phosphate (17), and consequently, lightning-generated calcium phosphite may have a significant role in biogenesis. The theory of lightning-induced reduction of phosphorus oxidation states is supported by recent measurements of phosphite in fulgurites, which are glasses formed by cloud-to-ground lightning (18).

However, sites of volcanic activity on modern Earth provide little evidence to support Gulick's theory. At present, only phosphates are known to be associated with volcanic rocks. However, Yamagata et al. (19) reported an occurrence of the phosphate dimer (pyrophosphate) and trimer (triphosphate) in fumaroles from Mount Usu, Shikotsu-Toya National Park, Hakkaido, Japan. The origin of these polyphosphates was attributed to hydrolysis of volatile P_4O_{10}. In contrast, thermodynamic equilibrium calculations suggest that reduced phosphorus gases, primarily PO_2, should dominate the phosphorus chemistry of fumaroles (20). As of yet, the redox state of volatile phosphorus in active volcanic environments remains unclear.

Geothermal vents are other sites influenced by volcanic activity on modern Earth. In these systems, groundwater comes in contact with hot water directly heated by magma in locations with high volcanic activity. The high temperatures and reducing conditions in geothermal vents could favor the formation of reduced phosphorus species. Pech et al. have detected phosphite and orthophosphate in Hot Creek Gorge, a geothermal vent near Mammoth Lakes, California (21). In this study, ion chromatography (IC), an established technique for the detection of phosphorus in aquatic systems (22,23) was coupled with suppressed conductivity detection to quantify phosphite and orthophosphate at concentrations of 0.06 ± 0.02 µM and 0.05 ± 0.01 µM, respectively, in aqueous samples from the geothermal vents (21).

Although IC with suppressed conductivity detection (IC–CD) is a highly sensitive technique, it is not highly specific. Any molecule that can form a negative ion will be separated and detected using IC–CD; however, ions of the same charge and similar size may have similar retention times (RTs), making it difficult to conclusively identify the compound of interest. Specificity can be enhanced by employing a mass spectrometer detector, which uses both RTs and unique mass-to-charge ratios to establish the identity of under-characterized compounds in complex systems. The current study couples IC to tandem suppressed conductivity and electrospray mass spectrometry (ESI-MS) detectors creating a highly sensitive and selective technique for the detection of phosphorus oxyanions in solution (24).

This paper expands on the previous successes of IC–CD and IC–ESI-MS as techniques for the quantitative and qualitative analysis of reduced phosphorus oxyanions in geothermal water to other matrices representative of cosmochemical and biological samples (21,24,25). Methods for the detection of hypophosphite (+1 oxidation state), phosphite (+3 oxidation state), orthophosphate (+5 oxidation state), hypophosphate (+4 oxidation state), and pyrophosphate (+5 oxidation state) are discussed. This list includes both reduced phosphorus oxyanions and polyphosphorus compounds, which are both important groups with respect to biogenesis. The chemical composition of various samples may interfere with the separation and/or detection of the analytes of interest. This paper will discuss techniques to minimize the impact of background ion interference and sample salinity on the detection of the five listed phosphorus oxyanions in natural water, synthetic cosmochemical, and biological samples. This study will enable investigators from the fields of chemistry, geochemistry, microbiology, agriculture, and environmental science to develop procedures specifically optimized to detect and quantify phosphorus oxyanions of choice.

Materials and Methods

Standards and calibrations

The instrument was calibrated from sodium salts solvated in aqueous solutions. The five sodium salts were sodium hypophosphite monohydrate (Sigma, 98%), sodium phosphite dibasic pentahydrate (Riedel-deHaën, 98%), sodium phosphate dibasic dihydrate (Riedel-deHaën, 99.5%), trisodium hypophosphate hexahydrate [synthesized using the methods of Yoza and Ohashi 1965 (12,26), and determined to be 97% purity by NMR], and tetrasodium pyrophosphate (VWR International, 98%). Nanopure 18 MΩ cm water (Barnsted, Dubugue) was used to solvate the phosphorus standards for the schreibersite and termite experiments. Standards in the geothermal water experiment were prepared in a matrix of synthetic geothermal water (24). This matrix was prepared in the laboratory from sodium salts to replicate the anion concentrations of all major anions present in Hot Creek reported in the literature (27), and observed in preliminary investigations (data not shown). The concentrations of background anions in the synthetic geothermal water calibration solution were 0.50 mM in fluoride, 6.0 mM in chloride, 5.9 × 10^{-3} mM in bromide, 4.1 × 10^{-5} mM in nitrate, 8.6 mM in hydrogen carbonate, and 1.0 mM in sulfate.

Synthetic schreibersite corrosion sample preparation

Pure iron phosphide (Fe_3P) powders (~0.5 g each, from CERAC, Inc., 40 mesh) were placed in glass vials flushed with nitrogen gas and solvated in distilled water, or "Instant Ocean" solutions (28). The solution salinities were 0%, 10%, or 100% of the salinity found in the modern ocean. The solution pH was adjusted to 4, 7, or 10 using sodium hydroxide (NaOH) and hydrochloric acid (HCl) to raise and lower the pH, respectively. Each of these samples (a total of 18 combinations of solutions and phosphide powder) was corroded twice at either room temperature or at 50°C over the course of one week using previously published methodologies (6). In contrast to prior studies, no effort was made to precipitate iron from solution either through the use of NaOH or sodium sulfide (Na_2S), hence all phosphorus measured was free in the solution.

Termite extract sample preparation

Living termite specimens (*Zootermopsis angusticollis)* were purchased from Ward's Natural Science and all termites were adults (≈ 34.5 mg/termite). The hindguts were extracted by using sterilized forceps and pooled in sterile microcentrifuge tubes. Nine milligrams was the typical yield from a single termite. By extracting 130 termites, a total of 1170 mg of extract was obtained. The collected hindgut extraction was diluted to five

times the initial volume using 18 MΩ cm Milli-Q water (Millipore, Billerica, MA) and further mashed to homogenous suspension. The turbid suspension was gently vortexed and then centrifuged at 7000 RPM for 60 s. The precipitate was discarded and the supernatant fluid was filtered through a 0.22 µm cellulose acetate filter and stored at –20°C prior to analysis. Defrosted samples were diluted a second time prior to analysis in 18 MΩ cm water yielding total dilution factors of 1:45 to 1:15 prior to sample analysis.

Geothermal water sample preparation

Water samples were collected from Hot Creek Gorge, an active geothermal pool located in a restricted access area near Mammoth Lakes, California on August 7, 2006. Geothermal pool samples were initially collected with a Teflon scooper (Waterra, UK) submerged approximately 1 m below the water surface. The collected water was transferred into 500-mL amber HDPE bottles. The scooper and bottles were rinsed onsite with water from the respective sampling site prior to sample collection. The samples were transported to a nearby field workstation and were filtered through 0.2 µm GTTP membrane filters (Millipore, Billerica, MA) using polysulfone field filtration units (PN 673-126, Nalgene). The filtered samples were immediately transferred to 125-mL amber HDPE bottles and were stored continuously at 4°C prior to analysis. In the laboratory, samples were pretreated with Dionex OnGuard II sulfonic acid cartridges and bubbled with UHP helium gas to remove excess carbonate from the samples prior to analysis. All samples were continuously stored at 4°C prior to analysis.

IC detection techniques

Full details of the IC–ESI-MS experimental methods can be found in Ivey and Foster (24). Highlights are presented here. Samples were injected into the IC (DX600, Dionex) using injection loops 15 or 700 µL in volume. The injection loop size was selected based on the projected concentration of total phosphorus in each sample. The IC was outfitted with an AS17 analytical column with a guard and electrolytically generated potassium hydroxide eluent (Dionex EG40). The suppressed conductivity detector data was collected for the entire runtime of the experiment. The effluent from the IC was pulsed into the mass spectrometer using an actuator valve at the rate of one pulse per s for time intervals selected to catch hypophosphite, phosphite, orthophosphate, hypophosphate, and pyrophosphate peaks without unnecessarily exposing the mass spectrometer to high concentrations of superfluous anions (i.e., chloride, carbonate, and sulfate). The mass spectrometer data was collected throughout the entire runtime, but the IC effluent was only directed into the mass spectrometer during the RT ranges of 0.1–2.8 min, 9.5–10.5 min, and 14.0–20.0 min for the schreibersite and termite studies. The phosphorus oxyanion RTs were significantly different in the geothermal water study that employed a large 700 µM injection loop. For this study, the effluent was analyzed by MS during RT ranges of 0.0–3.0 min, 5.5–8.0 min, and 13.0–15.0 min.

The ion trap mass spectrometer (LCQ Deca, ThermoFinnigan) configured with ESI operated with 5.4 kV on the needle, and the heated capillary tubing was held at 350.4°C. For the schreibersite corrosion and termite extract samples, 50:50 water–methanol mixture was delivered to the mass spectrometer by a Surveyor HPLC pump at a flow rate of 200 µL/min. For the geothermal water samples, pure 18 MΩ cm water was continually pumped by the HPLC pump into the mass spectrometer at a flow rate of 500 µL/min. The electrospray nozzle was placed as close as possible to the API transfer tube (Position 1), and the sheath gas was maintained at 83.35 (arbitrary units) (24). Mass spectra were collected for all samples using three consecutive single ion monitoring (SIM) experiments at $m/z = 65 \pm 1$, $m/z = 81 \pm 1$, and $m/z = 97 \pm 1$. The mass-to-charge ratio of 50 is the lowest that can be detected by the LCQ Deca mass spectrometer. Consequently, only singularly-charged hypophosphite, phosphite, and orthophosphate were detected in this study, although about 50% of phosphite and orthophosphate ions are doubly charged at near neutral pH. The list of consecutive SIM experiments was expanded to include $m/z = 161 \pm 1$, and $m/z = 177 \pm 1$ for the schreibersite sample study. The five phosphorus compounds monitored with IC–ESI-MS were hypophosphite ($H_2PO_2^-$), phosphite ($H_2PO_3^-$), orthophosphate ($H_2PO_4^-$), hypophosphate ($H_3P_2O_6^-$), and pyrophosphate ($H_3P_2O_7^-$), and these compounds were monitored at $m/z = 65$, $m/z = 81$, $m/z = 97$, $m/z = 161$, and $m/z = 177$, respectively.

Results and Discussion

IC and MS identification of phosphorus oxyanions

Figure 1A shows a typical ion chromatogram for five phosphorus oxyanions monitored using suppressed conductivity. The labeled peaks correspond to hypophosphite, phosphite, orthophosphate, hypophosphate, and pyrophosphate anions, each at concentrations of 200 µM, solvated in 18 MΩ cm water. The unlabeled peaks were produced by common anion impurities such as chloride, hydrogen carbonate, and sulfate (25). Separation was performed with an IC system that employed electolytically generated potassium hydroxide as the eluent. During the time of separation, the ions were in a very basic environment, and therefore, all of the acidic protons on these ions were deprotonated. Therefore, hypophosphite (Peak 1), which has only one acidic proton, had a charge of –1, and eluted at a very early RT. Phosphite (Peak 2), which had two acidic protons, had an RT close to that of carbonate (CO_3^{-2}, RT 10.8 min), which was present due to carbon dioxide dissolved in the aqueous solution. Orthophosphate (Peak 3), which had three acidic protons, eluted next. Both hypophosphate (Peak 4) and pyrophosphate (Peak 5) had four acidic protons, and therefore, were strongly retained by the column and had similar RTs. The peak assignments for the five phosphorus anions were determined by running each compound alone with the same method used to acquire the data (data not shown). Linear regressions fit to peak area versus concentration data were performed to calibrate all five phosphorus oxyanion salts solvated in 18 MΩ cm water, each at concentrations of 0.625 to 200.00 µM. The results are summarized in Table I.

After separation, the eluent stream was directed into the suppressor, where the alkaline hydroxide eluent was converted to pH-neutral water. Consequently, the phosphorus ions fully

deprotonated during separation, and re-equilibrated into the charge states present in neutral water solutions, as predicted from their thermodynamic equilibrium constants (pK_as). For example, phosphite would be found as both the singly-charged ion ($H_2PO_3^-$) and the doubly deprotonated species (HPO_3^{2-}) (29). CO_3^{2-} would be converted to hydrogen carbonate (HCO_3^-) at pH = 7. The neutral solution was diverted into the mass spectrometer, where the tentative identities of the ions were confirmed by ESI-MS (Figure 1B–F). Mass spectra were collected using consecutive single ion monitoring (SIM) experiments at m/z = 65 ± 1, m/z = 81 ± 1, m/z = 97 ± 1, m/z = 161 ± 1, and m/z = 177 ± 1. These mass-to-charge ratios correspond to the singly-charged ions of hypophosphite, phosphite, orthophosphate, hypophosphate, and pyrophosphate, respectively. Figure 1 shows that all five phosphorus oxyanions observed in the alkaline IC separation produce SIM signals that correspond to the singly-charged phosphorus oxyanion parent masses. The RTs observed in the SIM experiments match the RTs of the fully deprotonated phosphorus compounds observed in the conductivity data presented in Figure 1A. The only exception is hypophosphate (Peak 4), which produced an SIM signal at m/z = 161, which corresponds to the singly-charged ion, and an additional peak in the m/z = 177 spectrum. One possible explanation for this peak is the formation of a hypophosphate/oxygen atom adduct. High voltage was used to produce ions in these experiments. These experimental conditions enabled in-source collisional induced-dissociation (CID) of analytes, and made it possible to form oxygen atom daughter fragments from the parent analytes (30). Consequently, adducts such as the hypophosphate/oxygen atom adduct proposed here are likely. Therefore, both peaks, in conjunction with the IC RT, can be used to confirm the presence of hypophosphate in an unknown sample.

Table I. Ion Chromatography Peak Area Calibration Parameters for Phosphorus Oxyanions in 18 MΩ cm Water, Injected Using a 15 µL Injection Loop*

	Hypophosphite	Phosphite	Orthophosphate	Hypophosphate	Pyrophosphate
Range (µM)	0.625–200	0.625–200	0.625–200	0.625–200	0.625–200
R^{2}†	0.999	0.999	0.999	0.999	0.999
No. of Data points	6	6	6	6	6
Slope‡	2.00 ± 0.04	2.57 ± 0.05	2.81 ± 0.06	3.61 ± 0.07	5.7 ± 0.1
Intercept§	–9 ± 4	–9 ± 4	–15 ± 5	–21 ± 7	–26 ± 10
LOD (µM)	2.68	1.74	1.43	1.3	2.0

* The limits of detection were calculated as three times the standard deviation of measured baseline peak height variations in four separate 18.2 MΩ cm water samples.
† Linear regression coefficient
‡ (× 10^3 µS × min/µM)
§ (× 10^3 µS × min)

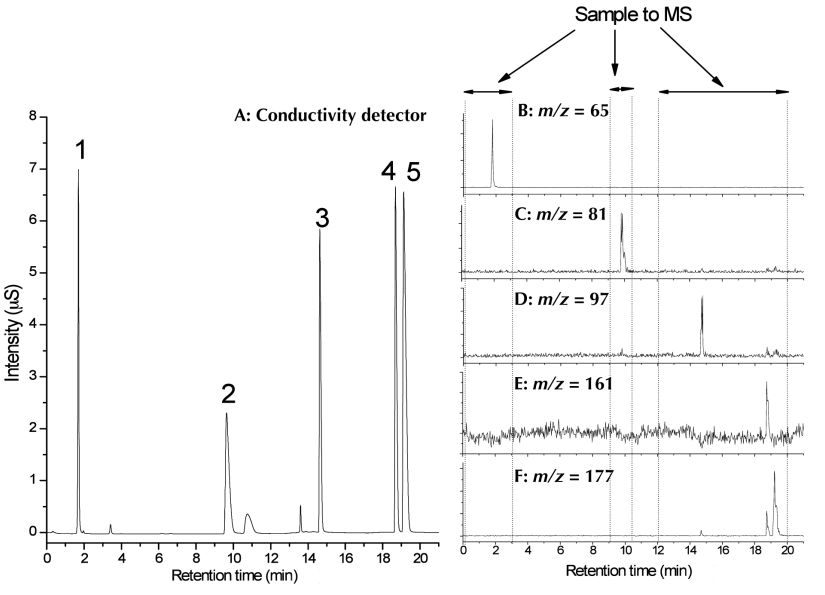

Figure 1. Ion chromatograms of five phosphorus oxyanion standards in 18 MΩ cm water analyzed with suppressed conductivity detection (A), and electrospray mass spectrometry single ion monitoring experiment detection (B–F). The phosphorus oxyanions are: 1, hypophosphite; 2, phosphite; 3, orthophosphate; 4, hypophosphate; and 5, pyrophosphate. The five consecutive single ion monitoring experiments were at m/z = 65 ± 1, m/z = 81 ± 1, m/z = 97 ± 1, m/z = 161 ± 1, and m/z = 177 ± 1, and are presented in panels B–F, respectively. The IC effluent was directed to the mass spectrometer only during time intervals bracketed between the dotted lines.

Synthetic schreibersite corrosion samples

Figure 2 presents representative chromatograms of a schreibersite corrosion sample solvated in distilled water (0% salinity) with a pH of seven. Samples were injected with a 15 µL injection loop. The solid line shows the sample, while the dotted line shows the same sample spiked with the five listed phosphorus oxyanions. Peak assignments were made based on the peak RTs for the reduced phosphorus oxyanions in the calibration standard (Figure 1) and the observed RTs in the spiked samples. The peak RTs of the phosphorus oxyanion standards are 1.7, 9.8, 14.7, 18.8, and 19.4 min, and were assigned to hypophosphite, phosphite, orthophosphate, hypophosphate, and pyrophosphate, respectively. The distilled water matrix in which the laboratory samples were prepared was ideal for identifying and quantifying phosphorus oxyanions. The conductivity detector data presented in Figure 2A contains only three significant background peaks, none of which interfere with the analytes.

ESI-MS serves as a selective detector, which is used here to confirm the assignment of unknown peaks in the schreibersite corrosion sample. Figure 2, Panels B, C, and D present representative chromatograms at m/z = 65 ± 1, m/z = 81 ± 1, and m/z = 97 ± 1, respectively, generated from SIM experiments using the ESI-MS detector. Additional chromatograms for m/z = 161 ± 1 and m/z = 177 ± 1 are presented in Supplement Figure 1. Each SIM chromatogram in Figure 2 contains a single, well-defined peak. The m/z = 65 signal in Figure 2B matches the RT of a singly-charged hypophosphite ion ($H_2PO_2^-$). The peak RT of

1.8 min is 0.1 min later than the observed hypophosphite peak in Figure 2A collected by the conductivity detector, which is reasonable based on the fact that the ESI-MS is the second detector in the series. Figure 2C contains a signal with a peak RT of 9.9 min observed at $m/z = 81 \pm 1$, in agreement with the assignment of Peak 2 as a singly-charged phosphite ion ($H_2PO_3^-$). The signal observed at 14.7 min in Figure 2D has a RT and a mass-to-charge ratio in agreement with the assignment of Peak 3 to orthophosphate ($H_2PO_4^-$). There is no activity in the $m/z = 161 \pm 1$ and $m/z = 177 \pm 1$ chromatograms (Supplemental Figure 1, Panels S1B and S1C, respectively) in the unspiked schreibersite corrosion samples, which indicates hypophosphate and pyrophosphate were not present in this sample above the limits of detection (LOD). The 3σ LOD were calculated as three times the standard deviation (SD) of the peak area in the blank runs and correspond to concentrations of 1.3 µM and 2.0 µM for hypophosphate and pyrophosphate, respectively. These results combined with the conductivity data previously mentioned herein are used to conclude that hypophosphite, phosphite, and orthophosphate are present in schreibersite corrosion samples solvated in pH = 7 distilled water, confirming prior results (31). Prior experiments have shown the presence of both hypophosphate and pyrophosphate in schreibersite corrosion experiments (4,6,12,31).

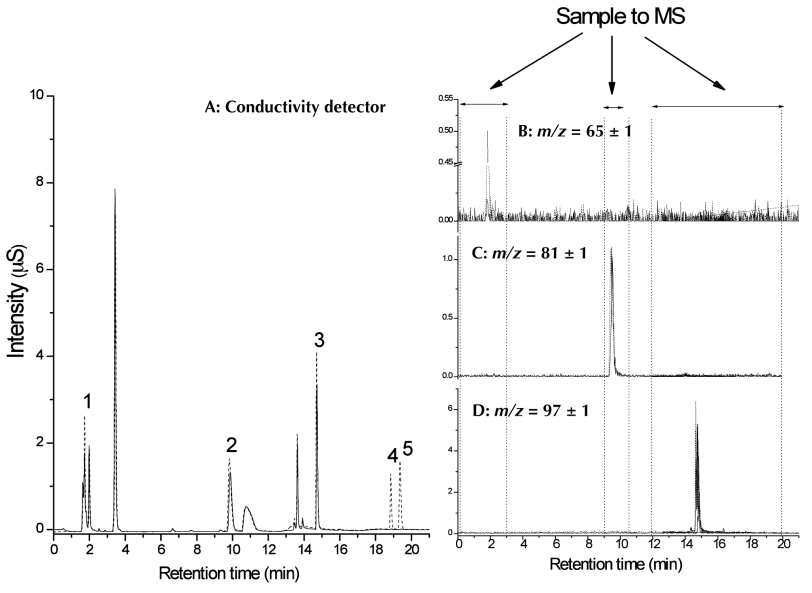

Figure 2. Representative chromatograms of the schreibersite corrosion sample (solid black line) and the same sample spiked with five phosphorus oxyanions (dashed line). The sample had pH = 7 and 0% salinity. The four panels present were (A) conductivity detector data; (B) single ion monitoring data at $m/z = 65 \pm 1$; (C) single ion monitoring data at $m/z = 81 \pm 1$; and (D) single ion monitoring data at m/z = 97 ± 1. The IC effluent was directed to the mass spectrometer only during time intervals bracketed between the dotted lines.

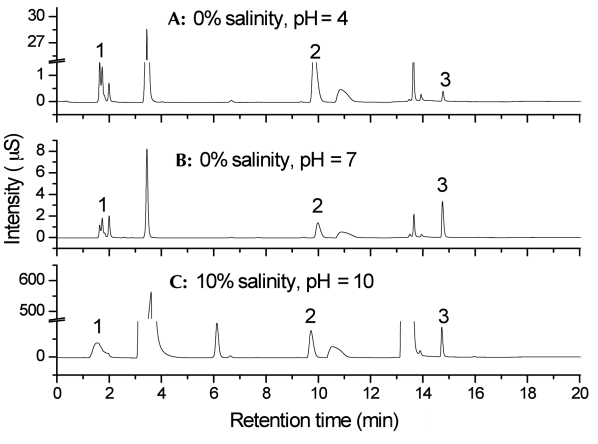

Figure 3. Representative chromatograms of acidic, neutral and alkaline schreibersite corrosion samples monitored using suppressed conductivity detection. Acidic (pH = 4) and neutral (pH = 7) samples presented in panels A and B, respectively, are in aqueous solutions with 0% salinity. The alkaline (pH = 10) sample is in a solution with a salinity equivalent to 10% of the salinity of the modern day ocean.

In previous studies of schreibersite corrosion, solutions were made alkaline by adding NaOH or Na_2S in order to precipitate iron compounds in solution for analysis by nuclear magnetic resonance. However, the process of changing the pH alters the solution composition, and may yield different results than corrosion samples that did not have a change in pH prior to analysis. In this study, samples were filtered to remove particulates, and the filtrate was analyzed using IC without further processing. One advantage of suppressed IC using a very basic eluent is that all of the phosphorus oxyanions were converted to their fully deprotonated forms immediately after injection, independent of the initial sample pH and charge state of each ion prior to injection. This characteristic enhanced the sensitivity of suppressed IC for the analysis of oxyanions because each oxyanion eluded at a single RT with the best signal-to-noise ratio possible. After IC analysis, the original pH of the solution and the pK_as of the fully protonated form could be used to calculate which forms of the ion were present in the solution.

Because the IC system utilized a very basic eluent, the analysis of schreibersite corrosion samples was not limited to pH = 7 samples in distilled water. Samples were prepared with a pH of 3, 7, and 10, which included both acidic and alkaline samples. Figure 3 presents the suppressed conductivity detector results for representative acidic, neutral and alkaline samples. The acidic (Figure 3A) and neutral samples (Figure 3B) were both solvated in pure water with 0% salinity. The alkaline sample (Figure 3C) had a salinity equivalent to 10% of the salinity of the modern ocean. Previous authors, employing extremely acidic or alkaline samples, recommended neutralizing prior to analysis using IC (32). However, neutralization was not employed in the current study and the analysis of both acidic and alkaline samples resulted in high-quality chromatograms.

Select synthetic schreibersite corrosion samples were solvated in solutions with salinities representative of 10% of the modern ocean. A representative chromatogram is presented in Figure 3C. The impact of increased salinity of the samples was not as easy to ignore. Saline samples can be difficult to flush from the injector between consecutive injections. This resulted in a carry over, which made it challenging to establish a consistent base-

line, and created peak shifting. Methods for the analysis of brine samples have been published (33); however, these methods were not applied in the current study. With the addition of salt at 10% of the modern ocean salinity, there was a decrease in the sensitivity of the IC–CD technique to hypophosphite. Hypophosphite was no longer resolved from background peaks in the sample. The sensitivity of the IC–CD technique to hypophosphite, which eludes from the column particularly early, was compromised by peak broadening that occurred when the total number of ions in the column increased (24).

In contrast to previous experiments, pyrophosphate and hypophosphate were not observed in the schreibersite corrosion samples analyzed by suppressed IC. Because these solutions were not made alkaline prior to analysis, both pyrophosphate and hypophosphate were likely bound to iron particles, and thus were excluded from the analysis. The present results also show that the release of phosphite is strongly dependent on temperature, and somewhat dependent on pH. Samples heated to 50°C show twice the phosphite of those samples corroded at room temperature. A higher pH also increased phosphite release by a factor of 40% from a pH of 4 to a pH of 7. Hypophosphite shows a similar change associated with pH, but its release is less temperature-dependent. Orthophosphate shows a significant solubility increase from a pH of 4 to 7, consistent with known binding effects with iron. Temperature changes did not have a consistent effect on phosphate concentrations.

Termite extract samples

Figure 4 presents representative chromatograms of a termite sample spiked with hypophosphite, phosphite, and orthophosphate salts (dotted line), and the same termite sample without added phosphorus (solid line). The conductivity detector results (Figure 4A) shows supernatant from thawed termite samples produces a chromatogram with peaks present at 1.9, 10.0 and 14.8 min. The 1.9, 10.0, and 14.8 min peaks are active in the $m/z = 65 \pm 1$, $m/z = 81 \pm 1$, and $m/z = 97 \pm 1$ SIM mass spectrometer experiments, presented in Figures 4B, 4C, and 4D, respectively. Figure 4 shows that each of the aforementioned peaks grew when hypophosphite, phosphite, and orthophosphate standards were added to the thawed termite supernatant. These data suggest the reduced phosphorus oxyanions hypophosphite and phosphite are produced in the termite hindgut along with the thermodynamically stable orthophosphate.

Peak areas from the conductivity data in the unspiked termite sample were used to determine the concentration in the termite supernatant. The estimated concentrations for hypophosphite, phosphite, and orthophosphate in the termite supernatant were 369 µM, 1.78 µM, and 490 µM, respectively. Because this particular sample was run only in duplicate, error bars for these data are not available. It is safe to conclude the actual concentrations of these compounds in the termite extract were either equal to, or less than, these values. Future experiments may use an internal standard to determine the efficiency of the extraction procedure and provide a more accurate measure of phosphorus oxyanions present in termites.

High concentrations of proteins in biological samples interfere with the separation of anions with IC because they typically have a high affinity to the analytical column, which reduces the number of sites available for the separation of analytes (32). Centrifugation and pressurized ultra-filtration through 0.22 µm filters are two excellent methods for the separation of proteins from the aqueous phase in biological samples. The aqueous supernatant collected from centrifuged samples contained only water-soluble compounds, phosphorus oxyanions and other anions of interest. Sample preparation techniques including centrifugation were successfully applied to human sera, another protein rich media, resulting in the detection of perchlorate at trace concentrations (34). In the current study, centrifuged samples were filtered by 0.22 µm syringe filters to reduce the concentration of bacteria that may compromise the stability of phosphorus anions. Centrifugation is an efficient, inexpensive, elegant sample preparation technique for biological samples prior to analysis with IC.

Geothermal water samples

The analysis of geothermal water samples is particularly challenging due to the high salinity and variety of background anions that may limit the ability of a user to resolve phosphorus oxyanions from other anions, especially when the relative concentrations vary over several orders of magnitude. Geothermal water samples typically have higher salinity than other natural fresh water samples (27,35,36). For example, the specific conductance of Hot Creek Gorge was measured as 1630 µS, which is more than eight times greater than that of a neighboring fresh water spring (35). Measured concentrations of fluoride, hydrogen car-

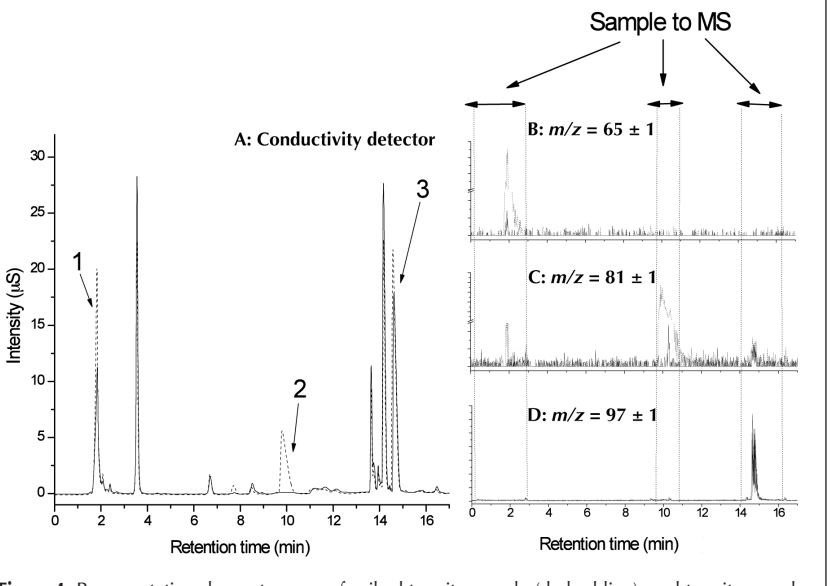

Figure 4. Representative chromatograms of spiked termite sample (dashed line), and termite sample (solid black line). The four panels present are (A) conductivity detector data; (B) single ion monitoring data at $m/z = 65 \pm 1$; (C) single ion monitoring data at $m/z = 81 \pm 1$; and (D) single ion monitoring data at $m/z = 97 \pm 1$. The IC effluent was directed to the mass spectrometer only during time intervals bracketed between the dotted lines.

bonate and chloride in Hot Creek Gorge were 0.51 mM, 9.0 mM and 6.3 mM, respectively (35). In comparison, the measured concentrations of fluoride, hydrogen carbonate and chloride in fresh water collected near the gorge were 0.032 mM, 1.8 mM, and 0.085 mM, respectively (35). The salinity of the geothermal vent sample is likely higher than the schreibersite corrosion samples in pure water and that of the supernatant of the termite extract.

Figure 5 shows the IC–CD and IC–ESI-MS results for a representative geothermal pool sample collected from Hot Creek Gorge on August 7, 2006. The following discussion focuses on the three labeled peaks produced by phosphorus oxyanions. The unlabled peaks are common anions including fluoride, chloride, hydrogen carbonate, and sulfate (21). The poor resolution observed in Figure 5A is consistent with typical behavior for an analytical column overloaded with ions. The manufacturer recommended 50 nanomole injection of any one analytes on the 4 mm Dionex IonPac AS17 analytical column (37). Loads as much as 7.2×10^3 times higher than the manufacturer's recommended capacity were injected onto the column during the analysis of Hot Creek Gorge samples. Chloride, hydrogen carbonate, and sulfate were all in violation of the manufacturer's recommended load capacity.

Peak 1 in Figure 5A has two local maximums consistent with two poorly resolved analytes. The analytes in Peak 1 are tentatively assigned as hypophosphite and fluoride. This assignment is based on a previous study by McDowell et al. that used the same column and smaller 15 µL injection loop to obtain a resolution of 1.52 between fluoride (1:4 dilution of synthetic geothermal water) and hypophosphite (25). The fluoride and hypophosphite concentrations in the McDowell et al. study were 108 µM and 20 µM, respectively (25). Like the other background ions in the McDowell et al. study, the concentration of fluoride was selected to mimic that which was observed in natural geothermal water. Resolving hypophosphite and fluoride with the Dionex IonPac AS17 was particularly challenging because of the poor affinity of these analytes to the column results in a short RT. The analysis of fluoride was further complicated by the fact that the presence of other ions in the sample caused these two peaks to broaden, because when the sample was initially loaded onto the column, all of the ions were competing for the same binding sites. As a result, poorly retained species, such as hypophosphite and fluoride, moved further down the column before they were eluded, resulting in those peaks becoming broader and poorly separated (24). Peak 1 in Figure 5 begins eluding at approximately 1.5 min, which does not leave much time for separation. The Dionex IonPac AG11-HC may be a better choice for resolving these anions based on the columns unique capability to retain small, singly-charged anions (38).

The limitations of IC coupled with conductivity detection for the detection of phosphorus oxyanions in complex, partially saline samples are apparent in the analysis of phosphite and orthophosphate, which were both undetectable by IC–CD in the geothermal water sample discussed here. Labels 2 and 3 in Figure 5A identify the approximate RTs wherein phosphite and orthophosphate are likely to elude based on previous experiments (21,24) and the IC–MS data presented in Figures 5B–5D. Results from the McDowell et al. study show that the resolution between phosphite and carbonate was 0.92, which is less than that obtained for hypophosphite and fluoride, despite the greater RT for the phosphite/carbonate ion pair (25). The large difference in the relative concentrations of these compounds may explain the poor resolution for the phosphite/carbonate ion pairs. Pech et al. measured a 0.06 ± 0.02 µM concentration of phosphite from the same geothermal vent one-year later, while typical background concentrations of hydrogen carbonate from this pool are 1.35×10^5 times higher than those measured in the adjacent stream (27). Consequently, it is likely that the combination of slight differences in selectivity factors, combined with the large difference in concentrations, resulted in the failure to detect phosphite in Figure 5. Unlike hypophosphite and phosphite, orthophosphate was predicted to elude without the interference of other anions. However, the concentrations in this sample are likely below the detection limit of orthophosphate, based on a comparison of these data to those reported by Pech et al. that showed orthophosphate concentrations are low in geothermal vent samples (21).

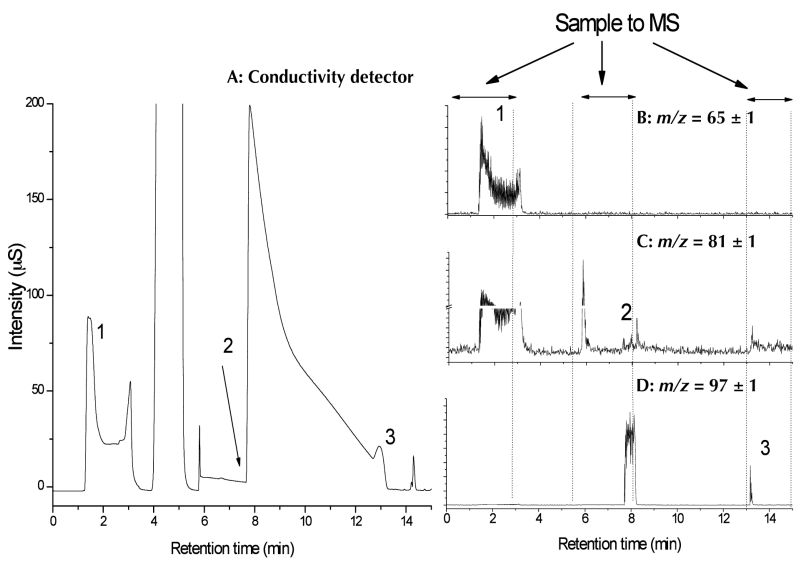

Figure 5. Representative chromatogram of geothermal water analyzed with suppressed conductivity detection (Panel A), and electrospray mass spectrometry single ion monitoring experiments at m/z = 65 ± 1, m/z = 81 ± 1, m/z = 97 ± 1 (Panel B–D). The IC effluent was directed to the mass spectrometer only during time intervals bracketed between the dotted lines.

A pulsed-injector valve was used to deliver IC effluent from the conductivity detector to the mass spectrometer in the time intervals 0.0–3.0, 5.5–8.0, and 13.0–15.0 min. These intervals were selected to capture potential hypophosphite, phosphite, and orthophosphate peaks in the geothermal pool sample, respectively. The m/z = 65 ± 1 signal presented in Figure 5B has approximately the same shape and RT as Peak 1, observed in Figure 5A. Unlike the conductivity detector, the ESI-MS detector has the ability to distinguish fluoride from hypophosphite. The singly-charged ions of fluoride and hypophos-

phite have mass-to-charge ratios of m/z = 19 and m/z = 65, respectively. Consequently, only hypophosphite would produce a signal under these experimental conditions because m/z = 50 is the smallest value that can be detected by this instrument. These data strongly suggest hypophosphite is present in geothermal hot springs. Due to the extremely large sample injection size, and the resulting column overload, it is feasible that fluoride and hypophosphite would be co-eluting, and therefore the broad, double peaked signal in the ion chromatogram is due to both species. From the IC–CD data alone, it would be impossible to confirm the presence of hypophosphite.

The result of the m/z = 65 ± 1 experiment must be reconciled with the observations in Figures 5C and 5D, which shows a pronounced signal at m/z = 81 ± 1. The shape and RT of this peak is similar to that observed in Figure 5B at m/z = 65 ± 1. One possible explanation is the formation of a hypophosphite/oxygen atom adduct. If fluoride was co-eluding with hypophosphite, the total ion count in the ionization region during analysis would have been high, and adduct formation would be certainly possible, especially in a matrix of fast-flowing, 100% water, where oxygen atoms are abundant (39).

Figure 5C presents the m/z = 81 ± 1 chromatogram of the geothermal pool. These data show one signal at 5.9 min, which co-eludes with a sodium bromide standard (data not shown). Bromine has two isotopes, m/z = 79 and 81, which occur in almost equal ratios. Even though phosphite and bromine have the same mass-to-charge ratio, the RT allowed the peak at 5.9 min to be identified as bromide. The only other features of the m/z = 81 ± 1 SIM trace are several very small peaks at 7.7–8.0 min, and one at 13.1 min. However, these peaks are barely above three times the standard deviation of the noise level, and therefore, by themselves, are not definitive identifications of phosphorus oxyanions. However, there is a large, broad peak that eludes between 7.7 and 8.0 min in Figure 5D with a m/z = 97 ± 1. As presented in the discussion of Peak 1, once again this experiment attempted to detect a trace concentration of phosphite in the presence of relatively large concentrations of a second ion, this time hydrogen carbonate. The electrospray formed from pure water droplets, with high total ion concentrations, high surface tension, high voltage on the needle, and a high flow rate of 500 µL/min. These conditions were less than ideal, and prone to results that are difficult to interpret. Under these conditions, in-source collisionally induced dissociation is highly probable and can result in the formation of both daughter ions and fragments rather than parent ions typically associated with ESI (30). The interpretation of these data may also be complicated by the formation of adducts that formed between the analytes and the background radicals and ions. In humid ion sources, such as the one employed in this study, oxygen radicals and ions are abundant (39). Therefore, it is feasible that the m/z = 97 ± 1 signal observed in the 7.7–8.0 min RT range is a phosphite-oxygen adduct. Although these data could not be used alone to identify an unknown, they may be used to support other experimental evidence. The addition of an organic solvent such as acetonitrile or methanol prior to ionization would certainly be advantageous. However, the challenges associated with saline samples must be considered in the analysis of all types of samples including natural water samples.

In conclusion, this study proved it is feasible to identify and quantify up to five different phosphorus oxyanions in aqueous samples in less than 20 min using suppressed IC equipped with tandem conductivity and ESI-MS detectors. These methods were successfully used to identify three of five phosphorus oxyanions in matrices representative of natural water, cosmochemical, and biological samples, and highlight a broader role for phosphorus redox chemistry in the environment than previously assumed. These ions include hypophosphite and phosphite, which are reduced phosphorus oxyanions linked to theories of biogenesis. Orthophosphate was also measured in each of the three media. In one case, sample preparation consisted only of dilution and filtration. Other samples required centrifugation or filtration with Dionex II OnGuard cartridges prior to analysis. These sample preparation techniques are simple, fast, and cost-effective procedures for the sensitive and selective analysis of phosphorus oxyanions. Large injection loops may be employed to enhance the sensitivity of analytes at low concentrations; however, data analysis may be complicated by column overload and ion-adduct formation. These techniques can be applied by investigators in a variety of disciplines including agriculture, food science, biogeochemistry, cosmochemistry, and in the biological and environmental sciences to elucidate the redox cycle of environmental phosphorus. This study shows a growing role for phosphorus redox chemistry in the natural world, and shows the role that IC may play in understanding the changes that occur in the environment to this biologically critical element.

Acknowledgments

This manuscript is based on an oral presentation presented at the 22nd International IC Symposium in Cincinnati, Ohio. The project described was supported by award numbers 1SC3GM083682-01 and 3SC3GM083682-02S1 from the National Institute of General Medical Sciences. The content is solely the responsibility of the authors and does not necessarily represent the official views of the National Institute of General Medical Sciences or the National Institute of Health. Support for TMS was provided by NSF-CREST program HRD-0932421. Support for LS was provided by NSF grant IOS-0920790. Support for MAP was from NASA Exobiology and Evolutionary Biology (grants NNX07AU08G and NNX10AT30G). Support for MGV was from the NSF-REU program award number CHE/0755567.

References

1. B. Schink and M. Friedrich. Phosphite oxidation by sulphate reduction. *Nature* **406:** 37 (2000).
2. B. Schink, V. Thiemann, H. Laue, and M.W. Friedrich. Desulfotignum phosphitoxidans sp nov., a new marine sulfate reducer that oxidizes phosphite to phosphate. *Arch. Microbiol.* **177:** 381–391 (2002).
3. A.K. White and W.W. Metcalf. Microbial metabolism of reduced phosphorus compounds. *Annu. Rev. Microbiol.* **61:** 379–400 (2007).

4. D.E. Bryant and T.P. Kee. Direct evidence for the availability of reactive, water-soluble phosphorus on early Earth. H-Phosphinic acid from the Nantan meteorite. *Chem. Commun.* **2006:** 2344–2346 (2006).
5. A. Gulick. Phosphorus as a factor in the origin of life. *Am. Scientist* **43:** 479–489 (1955).
6. M.A. Pasek and D.S. Lauretta. Aqueous corrosion of phosphide minerals from iron meteorites: a highly reactive source of prebiotic phosphorus on the surface of early Earth. *Astrobiology* **5:** 515–535 (2005).
7. G. Arrhenius, B. Sales, S. Mojzsis, and T. Lee. Entropy and charge in molecular evolution–the case of phosphate. *J. Theor. Bio.* **187:** 503–522 (1997).
8. R.O. Hallberg. Sediments: Their Interaction with Biogeochemical Cycles through Formation and Diagenesis, In *Global Biogeochemical Cycles*., S. Butcher, R.J. Charlson, G.H. Orians, and G.V. Wolfe, Eds. Academic Press: New York, NY, 1992.
9. R.A. Jahnke. The Phosphorus Cycle. In *Global Biogeochemical Cycles,* S.S. Butcher, R.J. Charlson, G.H. Orians, G.V. Wolfe, Eds. Academic Press: New York, NY, 1992.
10. W.H. Schlesigner. *Biogeochemistry: An Analysis of Global Change*. Academic Press, London, UK, 1991.
11. F.J. Stevenson. *Cycles of Soil: Carbon, Nitrogen, Phosphorus, Sulfur, Micronutrients*. John Wiley & Sons, Inc.: New York, NY, 1986.
12. M.A. Pasek, J.P. Dworkin, and D.S. Lauretta. A radical pathway for organic phosphorylation during schreibersite corrosion with implications for the origin of life. *Geochem. Comsochim. Acta* **71:** 1721–1736 (2007).
13. M.A. Pasek, T.P. Kee, D.E. Bryant, A.A. Pavlov, and J.I. Lunine. Production of potentially prebiotic condensed phosphates by phosphorus redox chemistry *Angew. Chem., Int. Ed. Engl.* **47:** 7918-7920 (2008).
14. D. Glindemann, M. Edwards, and P. Morgenstern. Phosphine from rocks: Mechanically driven phosphate reduction. *Environ. Sci. Technol.* **39:** 8295–8299 (2005).
15. D. Glindemann, M. Edwards, and O. Schrems. Phosphine and methylphosphine production by simulated lightning–a study for the volatile phosphorus cycle and cloud formation in the earth atmosphere. *Atmos. Environ.* **38:** 6867–6874 (2004).
16. R.M. DeGraaf and A.W. Schwartz. Reduction and activation of phosphate on the primative earth. *Origins Life Evol. Biosphere* **30:** 405–410 (2000).
17. D. Glindemann, R.M. DeGraaf, and A.W. Schwartz. Chemical reduction of phosphate on the primative earth. *Origins Life Evol. Biosphere* **29:** 555–561 (1999).
18. M. Pasek and K. Block. Lightning-induced reduction of phosphorus oxidation state. *Nature Geoscience.* **2:** 553–556 (2009).
19. Y. Yamagata, H. Watanabe, M. Saitoh, and T. Namba. Volcanic production of polyphosphates and its relevance to prebiotic evolution. *Nature* **352:** 516–519 (1991).
20. V.S. Mambo, M. Yoshida, and S. Matsuo. Partitioning of arsenic and phosphorus between volcanic gases and rock. Part 1. Analytical data and magmatic conditions at Mount Usu, Japan. *J. Volcan. Geotherm. Res.* **46:** 37–47 (1991).
21. H. Pech, A. Henry, C.S. Khachikian, T.M. Salmassi, G. Hanrahan, and K.L. Foster. Detection of geothermal phosphite using high performance liquid chromatography. *Environ. Sci. Technol.* **43:** 7671–7675 (2009).
22. P.R. Haddad, P.N. Nesterenko, and W. Buchberger. Recent developments and emerging directions in ion chromatography. *J. Chromatogr., A* **1184:** 456–473 (2008).
23. V. Ruiz-Calero and M.T. Galceran. Ion chromatographic separations of phosphorus species: A review. *Talanta* **66:** 376–410 (2005).
24. M.M. Ivey and K.L. Foster. Detection of phosphorus oxyanions in synthetic geothermal water using ion chromatography–mass spectrometry techniques. *J. Chromatogr., A* **1098:** 95–103 (2005).
25. M.M. McDowell, M.M. Ivey, M.E. Lee, V.V.V. Firpo, D. Salmassi, C.S. Khachikian, and K.L. Foster. Detection of hypophosphite, phosphite, and orthophosphate in natural geothermal water by ion chromatography. *J. Chromatogr., A* **1039:** 105–111 (2004).
26. N. Yoza and S. Ohashi. Oxidation of red phosphorus with hydrogen peroxide and isolation disodium dihydrogen hypophosphate. *Bull. Chem. Soc. Japan* **38:** 1408–1409 (1965).
27. L. Eccles. Sources of arsenic in streams tributary to Lake Crowley, CA. Water Resour. Invest. 76–36 (1976).
28. J. Edmund and J. Mowka. The SeaWater Manual: Fundamentals of Water Chemistry for Marine Aquarists; Instant Ocean, 2009.
29. G. Hanrahan, T.M. Salmassi, C.S. Khachikian, and K.L. Foster. Reduced inorganic phosphorus in the natural environment: Significance, speciation and determination. *Talanta* **66:** 435–444 (2005).
30. A.W.T. Bristow, W.F. Nichols, K.S. Webb, and B. Conway. Evaluation of protocols for reproducible electrospray in-source collisionally induced dissociation on various liquid chromatography/mass spectrometry instruments and the development of spectral libraries. *Rapid Commun. Mass Spectrom.* **16:** 2374–2386 (2002).
31. D.E. Bryant, D. Greenfield, R.D. Walshaw, S. Evans, A.E. Nimmo, C. Smith, L. Wang, M.A. Pasek, and T.P. Kee. Electrochemical studies of iron meteorites. Phosphorus redox chemistry on the early Earth. *Int. J. Astrobiol.* **8:** 27–36 (2009).
32. J. Weiss. Handbook of Ion Chromatography; 3rd ed.; Wiley-VCH Verlag GmbH & Co. KGaA, Weinheim: Verlag, Germany, 2004; Vol. 1.
33. P.F. Kehr, B.A. Leone, D.E. Harrington, and W.R. Bramstedt. *LC-GC* **1118:** (1986).
34. C. Reiter, S. Müller, and T.J. Müller. *Chromatogr.* **413:** 251 (1987).
35. R.H. Mariner and L.M. Willey. Geochemistry of thermal waters in Long Valley, Mono County, California. *J. Geophys. Res.* **81:** 792–800 (1976).
36. M.L. Sorey. Evolution and present state of the hydrothermal system in Long Valley Caldera. *J. Geophys. Res.* **90:** 11219–11228 (1985).
37. Dionex IonPac AS17 Manual; Dionex Corporation: Sunnyvale, 2002.
38. Dionex Product Manual: IONPAC AG11-HC Guard Column; IONPAC AS11-HC Analytical Column, Revision 06; Dionex Corporation, 1997-2004, 2004.
39. D. Vogt. Über Die Energieabhängigkeit Und Den Mechanismus Von Reaktionen Bei Stössen Langsamer Negativer Ionen Auf Moleküle. *Int. J. Mass Spectrom. Ion Phys.* **3:** 81–90 (1969).

Manuscript received December 1, 2010;
revision received April 4, 2011.